Bangor University

MASTERS BY RESEARCH

High Entropy Alloys and Their Desirability For Novel First Wall Materials In Fusion Applications

Lin-Vines, Alexander

Award date:
2022

Awarding institution:
Bangor University

[Link to publication](#)

School of Computer Science and Electronic Engineering
College of Environmental Sciences and Engineering

High Entropy Alloys for First Wall Fusion Applications

Alexander Lin-Vines

Submitted in partial satisfaction of the requirements for the Master by Research

Supervisor Dr. Simon S.C. Middleburgh

February 2021

Acknowledgements

I would like to thank my Mother and Father for the continuous support throughout my life to get me to be proud of who I am today. My British Grandparents for always believing in me. My Chinese Grandparents for inspiring me and showing me how to follow my dreams. I will forever appreciate my partner for being by my side supporting me no matter the difficulty.

Statement of Originality

I hereby declare that this thesis is the results of my own investigations, except where otherwise stated. All other sources are acknowledged by bibliographic references. This work has not previously been accepted in substance for any degree and is not being concurrently submitted in candidature for any degree unless, as agreed by the University, for approved dual awards.

Student:

Alexander Lin-Vines

Yr wyf drwy hyn yn datgan mai canlyniad fy ymchwil fy hun yw'r thesis hwn, ac eithrio lle nodir yn wahanol. Caiff ffynonellau eraill eu cydnabod gan droednodiadau yn rhoi cyfeiriadau eglur. Nid yw sylwedd y gwaith hwn wedi cael ei dderbyn o'r blaen ar gyfer unrhyw radd, ac nid yw'n cael ei gyflwyno ar yr un pryd mewn ymgeisiaeth am unrhyw radd oni bai ei fod, fel y cytunwyd gan y Brifysgol, am gymwysterau deuol cymeradwy.

Statement of Availability

I hereby acknowledge the availability of any part of this thesis/dissertation for viewing, photocopying or incorporation into future studies, providing that full reference is given to the origins of any information contained herein. I further give permission for a copy of this work to be deposited with the Bangor University Institutional Digital Repository, and/or in any other repository authorised for use by Bangor University and where necessary have gained the required permissions for the use of third-party material. I acknowledge that Bangor University may make the title and a summary of this thesis/dissertation freely available.

Student:

Alexander Lin-Vines

ABSTRACT

High entropy alloys (HEAs) are increasingly studied for nuclear applications due to their unique combination of desirable properties including radiation resistance that are straightforward to tailor. In this study, we investigated intrinsic defect formation in the equiatomic BCC MoNbTaVW HEA by means of density functional theory, the goal being to assess its response to radiation damage in its possible use as plasma facing material in future nuclear fusion devices. We show that when interstitial defects were considered, a clear preference for the formation of split interstitial defects is observed. Vanadium was the most common interstitial defect species after relaxation and most favourable when incorporated into split interstitial defects, often forming when other interstitials elements were initially placed within the structure. The results are rationalized based on the physical properties of the different elements.

Table of Contents

Table of Figures

Table of Tables

1. Introduction

The first publications reporting high entropy alloys (HEAs) were submitted nearly 2 decades ago, resulting in a range of new efforts in materials science and engineering for their potential application to a wide range of functional and structural components [1]. According to Yeh *et Al.* [1], a HEA is an alloy that contains at least 5 metallic elements (N≥5), each with concentration between 5-35 atom percent [2], [3], although there is a great degree of flexibility related to this description in the literature. It is suggested that disordered solid solutions remain stable relative to the ordered compounds in alloys because of the high entropies of mixing (ΔS_{mix}) [4]. The use of a high entropy alloy allows for more complex and tailored compositions for the desired properties in any application. The material in this study is expected to be used as the first wall material within a tokamak reactor and must be able to withstand a variety of hostile conditions.

A spherical tokamak reactor, first designed in mid -1980s, had shown promise in its importance for fusion power development [5]. The desirable features of high aspect ratio tokamaks while staying relatively small and inexpensive (when compared to traditional shape), show beneficial properties like operation at high beta [6]. High-β plasmas favour hydrodynamic pressure as the dominant force within the system meaning the ratio of plasma is higher to the magnetic pressures. Having a high-β plasma allows for more kinetic stabilising of the system. The fusion gain factor is the ratio of fusion power produced to power needed to maintain steady plasma within the reactor. Recent advances in tokamak physics and superconductor technology have allowed for relatively small spherical tokamaks (ST) considered possible to operate at high fusion gain. The key for high fusion gain with smaller spherical tokamaks are the technological advances in high-temperature super conductions (HTS). This is especially favourable with high-β plasma as the plasma is more magnetically confinable at lower aspect ratios [7].

With advances in understanding of tokamak scaling laws, it has been proven that that fusion gain relative to tokamak size is relatively low where the level of energy confinement is the most prominent factor [8, 9]. The use of high performing HTS have allowed for greater energy confinement for this reason. However, the essential components for ST operation must be protected. The HTS tapes within the core of the central column is a vital part of a tokamak. With high energy neutron radiation produced from the plasma, a material must be engineered to protect itself from damage.

The material required for the first wall must be able to withstand this long-term neutron irradiation and extreme heat as well as transient loading from plasma instabilities while keeping radiation waste to a minimum [10]. Neutron irradiation can cause damage to a material by creating defects in the atomic structure. With a material that can withstand the harsh fusion environment long-term, the capability to maintain its integrity extends its peak performance for longer with minimal degravitation. The combination of high field and small devices has opened the promising opportunity for developing spherical tokamaks for fusion energy sooner if the device is self-preserving long-term.

2. Literature review

2.1 Reactors

Over several decades, research groups have been advancing research into controlled nuclear fusion. The design of fusion reactors has resulted in distinctly different designs, aiming to surpass the breakeven point of energy in, to energy produced. With the use of supercomputers to understand the behaviour of fusion and the materials needed for them, research is continuing to break boundaries to make fusion reality.

2.1.1 Magnetic-Confinement Fusion (MCF)

Confinement of the place within a circular "donut" shaped reactor using superconducting magnets called a tokamak. These magnets are used to confine the plasma that's used to initiate and sustain fusion. Since 1960, there has been over 200 successfully built and functioning tokamaks with well-established supporting plasma physics fundamentals.

2.1.2 Stellarator

This interesting design shows a complex externally applied electromagnet surrounding a ribbon like fusion chamber similar concept used in MCF. This design produces high-density plasma that is shown to be more symmetrical and stable compared to a spherical tokamak which allows for this design of reactor to run longer. However, because of the complex design of this reactor, the geometry leaves the reactor extremely sensitive to imperfections.

2.1.3 Inertial-Confinement Fusion (ICF)

Using pulsed laser or ion beams, compression of the fuel pellets to extremely high densities create shock waves that heat plasma before dissipation. However, this method of fusion has shown difficulty in stabilising the laser-plasma exerted on the fuel which produces high-energy electrons that caused the fuel to break and scatter before fusion. The centimetre-sized hohlraum fuel pellets have laser beams fired into them that produce x-rays which ablate off the surface. Due to the complexity of the lasers, this reactor is extremely expensive to produce compared to other designs.

2.1.4 Magnetized Target Fusion (MTF)

The approach to this reactor design is a hybrid idea of both magnetic fields to contain the low-density plasma (similar to spherical tokamaks) and the use of compression from inertial confinement such as lasers or pistons. This method is still in early development as research is yet to find a way to increase the plasma density. Atoms must be under enough pressure and temperature in-order to fuse and create the hot plasma. The energy from the plasma is used to heat water to turn a turbine that's converted into electricity. However, the low-density plasma isn't dense enough to be useful or stable enough to maintain for a long period of time to allow the fuel to fuse. This means it's hard to generate enough energy to overcome the energy needed to start the fusion reaction.

2.1.5 Field-Reversed Configuration (FRC)

Containing the plasma within its own magnetic field, this reactor design uses a toroidal electric current inside of a cylindrical plasma. Unlike the direction of an externally supplied magnetic field, the axel field inside the reactor is reversed from eddy currents within the plasma [11]. TAE Technologies use this design of reactor where they use plasma guns to accelerate two plasmas into each other while heating them with a particle beam. Although this design of

electromagnets has shown to be less prone to instabilities compared to other reactor designs, researchers have not yet successfully produced dense or stable enough plasma for fusion.

There are three trends of fusion evolution shown in fig 1. The first being the progressive increase of tokamak dimensions with a parallel increase of plasma heating power. The second trend was the transition from traditional tokamaks with circular cross-section to an elongated plasma configuration that used poloidal magnetic diverters.

This design was first suggested by Artsimovich and Shafranov in 1972 ('Tokamak with non-round section of the plasma loop'[12]). With the third trend that illustrated the gradual transition from high-Z materials (SS, Mo, W) which was used as the material of the first wall and diverters- to materials with low Z (C, B, Be, Li). This transition was due to the hard pressure of experimental facts and hard resistance from engineers who preferred refractory metals compared to graphite, beryllium and lithium.
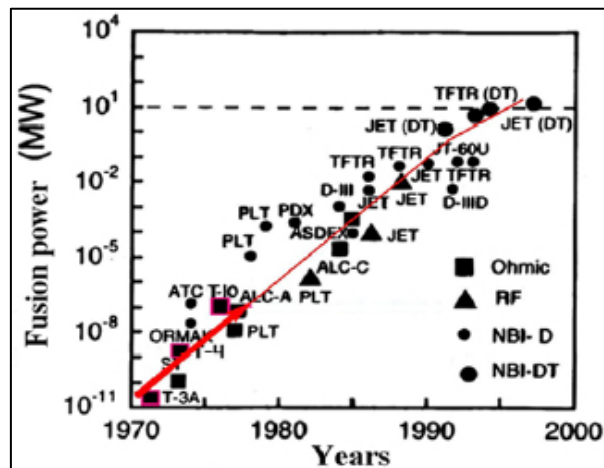
Figure 1 The evolution of the power of neutron- yield worldwide obtained through tokamak investigations 1971-1996 [15]. Temporal dynamics of fusion power output in high performance shots of tokamaks (PPPL), arrow–'Artsimovich vector' [16] from T-3 to T-10.

2.2 First wall Materials

Desirable properties for nuclear fusion first wall plasma facing shielding materials must yield high melting temperatures, thermal conductivity, low sputtering erosion rates and small tritium retention. Tungsten followed more recently where strong cooling of the central plasma was first observed in the PLT tokamak using this metal as a limiter [13]. Challenges arise to meeting first wall target lifetimes when in contact with a tokamak's burning plasma. There is demanding material erosion with continuous neutron and ion radiation that cause defects and impurities creating waste deposits and changes to composition. One of the main advantages of tungsten is its low permanent hydrogen retention [24] at elevated temperatures. Due to the higher atomic mass, substantial sputter by deuterium in the fuel occurs only at relatively high energies (e.g., sputtering rate 10-3 for 400eV ions) so that sufficiently cold deuterium plasma does not lead to substantial erosion [15]. The concern is widely recognised from the concentrated research efforts in place to develop a material within the tokamak industry comprising of wide varieties of compositions and plasma configurations to produce a suitable long-term material [16].

The JET reactor shows use of strong co-deposition of tritium with carbon [17] with their results of design studies of fusion reactors [18] has shown confidence in long term use of tungsten as the favoured material for plasma facing components [15]. JET was also seen to have used beryllium in 2009 when they proposed use in ITER. JET now uses tungsten for the diverter which will also be used in the ITER. Looking at Germany's second largest fusion project, tungsten is also used for the first wall in the ASDEX upgrade [19]. Arguably, it has also been proven that the addition of liquid lithium has various desirable properties that has suitable fusion reactor performance [20]. The Princeton Plasma Physics Laboratory reported that due to its chemical reactiveness, the ~0.02g of lithium coating of the PFCs resulted in the fusion power output of nearly a factor of two when it was used in TFTR [20].

With tungsten commonly recognised as the most suitable first wall material, noticeable radiation damage from He^+ ion implantation leads to the formation of internal blistering [21]. Bisters were forming from room temperature to 873 K for He^+ fluence range of 10^{21} to 4×10^{22} m^{-2} at energy range of 200 eV to 8 keV [21]. Another source of damage is the erosion from fast particles from additional heating. Fast deuterium ions that are generated by the Neutral Beam Injection can be lost from drifts of Magnetohydrodynamic (MHD)-effects [22].

2.2.1 Point defects in Compounds

Material damage can be described by looking at the any irregular arrangements within a lattice often described as a point defect. This can include self-interstitial atoms, interstitial impurity atoms, substitutional atoms and vacancies [21]. A self-interstitial atom is an additional atom that has forced its way into an interstitial void in the crystal structure.
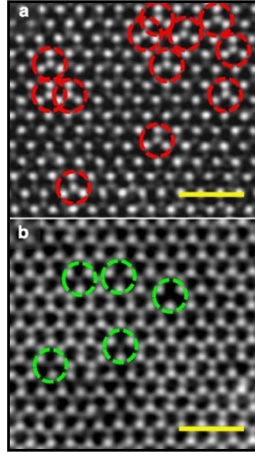
Figure 2 Point defects in PVD MoS2 monolayers. [74]

Self-interstitial atoms occur only in low concentrations within a lattice because they distort and highly stress the tightly packed lattice structure (fig 2).

A substitutional impurity atom is a different type of atom compared to the bulk atoms which has replaced one of the bulk atoms within the lattice structure. Substitutional impurity atoms are usually close in size (15%) to the rest of the atoms. An example is the zinc atoms in brass. The zinc atoms, which have a radius of 0.133 nm, would have replaced some of the copper, atoms which have a radius of 0.128 nm (<15%).

Interstitial impurity atoms are much smaller than the atoms in the bulk matrix. These atoms fit into the open space between the bulk atoms of the lattice structure. An example atom would be the carbon atoms added into iron to make steel. The carbon atoms with a radius of 0.071 nm fit between the open spaces in the larger 0.124nm iron atoms.
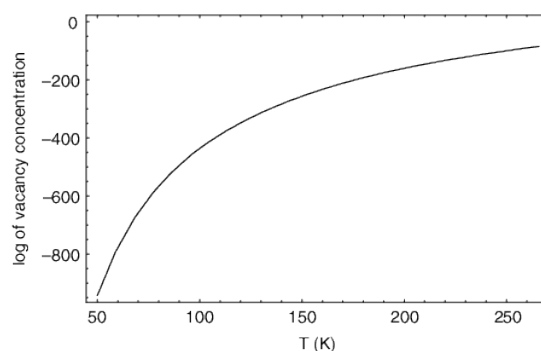
Figure 3 Positive correlation of vacancy concentration and temperature. [23]

A vacancy is an empty space where an atom should be. This missing atom is found commonly in high temperatures where atoms are frequently and randomly changing their positions, which leaves empty lattice sites shown in fig 3 [23]. In most cases, diffusion can only occur because of the vacancies. Typically, the displaced atom is ejected from its initial lattice site, forming an interstitial, and leaving a vacancy [14], known as a Frenkel pair. The energy can be transferred further into the material creating a cascade effect of damage from the initial impact of neutron irradiation.

2.3 High Entropy alloys

HEAs are seen to have increasingly more potential for nuclear fusion applications due to their mix of extraordinary properties like high strength-to-weight ratio and high hardness comparable to ceramics [24], fracture toughness and tensile strength [25], corrosion resistance [83] and radiation resistance [26]. HEAs were originally defined for containing at least 5 different elements, each with concentration between 5-35 atom percent [1, 2, 4]. However, the definition has loosened in recent years as to include both 4 element alloys and those with concentrations of elements greater than 35% [1]. Additionally, alloys possessing more than one solid-solution phase has also been referred to as high entropy alloys [1]. The high configurational entropy of HEAs significantly reduce the free energy of a system as temperature increases resulting in great high-temperature thermodynamic stability and highlighting their potential in high-temperature applications. The use of a high entropy alloy allows for more complex and tailored properties fit for a particular application.

Since the advent use of Ti/W metals in structural materials was depleting base elements, creating alloys became increasingly harder and more expensive. Fig 4 shows how high entropy alloys have exceptionally higher fracture toughness and high yield strength when compared to other conventional materials leading them to become a much more popular material of choice.
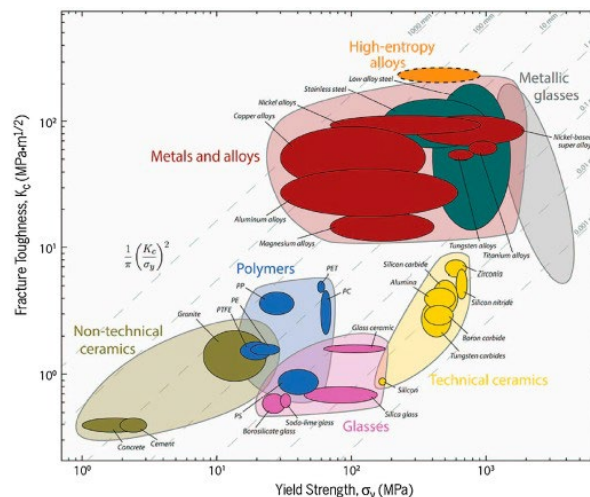
Figure 4 Fracture toughness vs. yield strength of most popular structural material types. [75]

2.3.1 High Entropy Alloy (HEA) Theory

The introduction of engineered HEAs has allowed for relatively stabilized solid-solution phases from their significantly high entropy mixing when compared to conventional intermetallic compounds and alloys, especially at higher temperatures [3] Conventional alloys are based on a single principal element which are usually optimised by alloying it with additional elements. This creates limitations on the material to the properties of the principal element. HEAs however, benefit from the varied concentrations of different elements thus leaving no bounds to this limitation.

Considering an equimolar alloy at its liquid or solid state, its configurational entropy per mole can be calculated using Boltzmans hypothesis on the relationship between entropy and complexity of a system [3]. This is shown by:

$$\Delta S_{conf} = -k \ln w = -R\left(\frac{1}{n}\ln\frac{1}{n} + \frac{1}{n}\ln\frac{1}{n} + \cdots + \frac{1}{n}\ln\frac{1}{n}\right) = -R\ln\frac{1}{n} = R \ln n \qquad \text{Eq (1)}$$

where R is gas constant, 8.314 J/K mol, and n is the number of elements [3].

Total mixing entropy is made up of four parts configurational, vibrational, magnetic dipole, and electronic randomness. With HEAs, configurational entropy is the main contribution [27], [28] Table 1 showing the configurational entropies of equimolar alloys that have a gas constant of R, shows how the entropy increases as the number of elements increases. When considering Richard's rule when there is an entropy change per mole, ΔS_f form solid to liquid state when melting is roughly one gas constant R for metals. It's also worth noting that the enthalpy changes or the latent heat per mole, ΔH_f can be correlated directly with ΔS_f by the equation $T_m\Delta S_f = \Delta H_f$. Due to ΔH_f regarded as the energy required to break around 1/12 of all bonds within a solid, the mixing entropy of R per mole from mixing in an alloy state would be high in order to decrease the mixing free energy by a certain amount of RT when at high temperatures [3]. For example, $RT = 8.314$ kJ/mol at 1000 K shows how much energy is required to decrease the mixing free energy while also competing with the mixing enthalpy of the intermetallic compounds found from the interactions between dissimilar metallic atoms. This leads to the tendency for the mixing state of constituent elements to be increased when increasing the mixing entropy.

Table 1 Configurational entropies of equimolar alloys with constituent elements up to 13 [3]

n	1	2	3	4	5	6	7	8	9	10	11	12	13
ΔS_{conf}	0	0.69R	1.1R	1.39R	1.61R	1.79R	1.95R	2.08R	2.2R	2.3R	2.4R	2.49R	2.57R

To illustrate entropy differences between high and low temperature states, HEA-1 is a single-phase solid solution over the full temperature range and a binary compound form in HEA-2 at Trxn Trxn (fig 5). HEAs are defined here by the magnitude of ΔS_{conf} in the high temperature state [4].
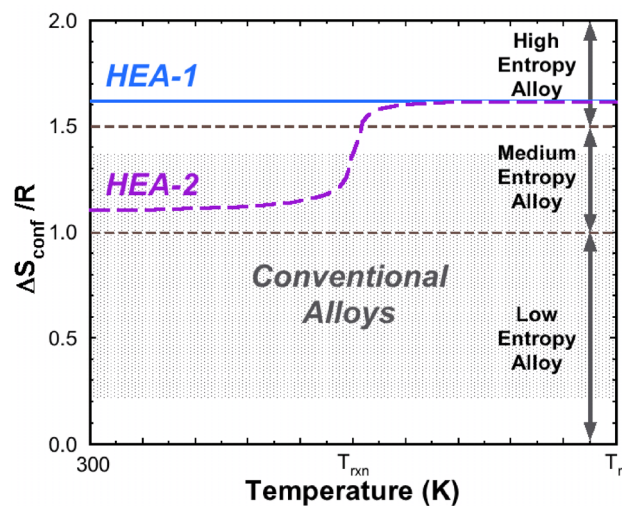

Figure 5 Illustrating entropy differences between high and low temperature states. [4]

From the single-phase HEA approach, the solid solution strengthening is more effective than with conventional alloys [2]. However, the potential for HEA solid solution strengthening has not been sufficiently studied for its extended loading times and temperatures above $T_m/2$. Gibbs phase rule states that in order to make HEAs have enough mixing entropy form simple single phase solid-solutions rather than complicated intermetallic compounds, HEAs are often designed to be equiatomic in order to maximise the mixing entropy. When considering the high entropy effect, solid solutions are easier to produce than intermetallics at the solidification process in HEA [3, 38 – 42]. Yet, the greatest benefit of HEAs is the high number of possible compositions available to study for more complex alloys. With single phase materials, there is still consideration for its grain size, shape and orientation that can all play a part in the final properties of the material [4] which can lead to the need for second phases. This process is useful for when structural loads are low, and the application temperature is below half of the absolute melting temperature ($T_m/2$) or when the criteria require low costs or to form environmental resistance [4]. Yet, there is a limited amount of single phase, solid solution conventional alloys that meet these requirements. 3xxx and 5xxx aluminium alloys (manganese and magnesium respectively) are strengthened by solid solution hardening and cold work, which are non-heat treatable and strain hardened only. These aluminium alloys work better in extreme temperatures due to the manufacturing process creating a harder material with area reduction being the main feature [34]. There can be an additional stage for "stabilising" which ensures that the final mechanical properties do not change over time. The use of alpha/near-alpha titanium alloys used in cryogenic and elevated temperatures are commonly utilised in the aerospace industry. Austenitic SS (Fe-C-Ni) with its strong environmental resistance are well known for its alloys 304 and 316 SS. "Solid solution strengthened Ni-based, and Fe-Ni based superalloys are used where formability is important, or when solution treatment, quench and ageing needed is impractical such as complex-shaped castings" [4].
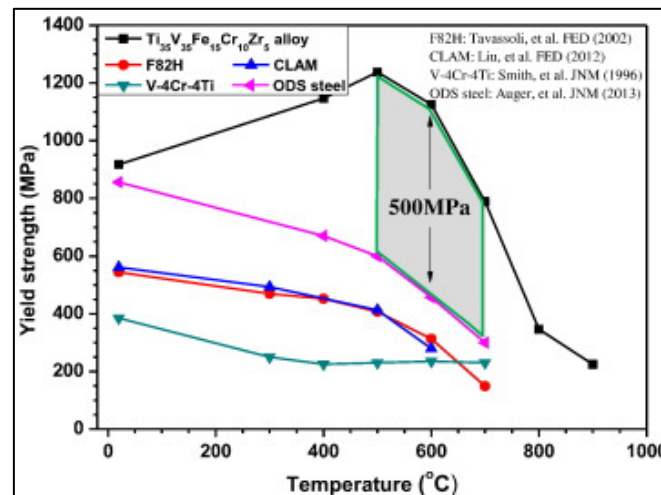
Figure 6 Comparison of yield strength for V35Ti35Fe15Cr10Zr5 alloy and low activation alloys from room temperature to 900 °C [38]

The differences shown in fig 6 in yield strength were questioned whether they attributed to the differences in microstructure of the alloys. The improved yield strength of the HEA appears to be caused from the effectiveness of strong solid solution and lattice distortion for strengthening of the HEA [29–31]. The strengths of low activation alloys show in fig 6 could be from the fine grain size and heat-treated alloys where the HEA was as-cast [38]. With a series of positive results for yield strength and activation of this HEA, the grain size measurements were not

measured. This creates a level of uncertainty for the true performance of the HEA compared to the alloys. However, the differences between the HEA and alloys were relatively large leading to confidence in the greater performance of the former.

With desirability for low-activation and high yield strength in materials for fusion applications beyond 700 °C, created the growing need to develop a new shielding material that can provide greater performance than tungsten or conventional alloys [38]. High entropy alloys that can provide the necessary properties at higher temperatures show suitability as first wall materials. Fabrication of a HEA $V_{35}Ti_{35}Fe_{15}Cr_{10}Zr_5$ by vacuum arc melting by Xian *et al.* and the microstructure of as-cast and annealed sample was found to be composed of BCC solid solution phases. The base materials were chosen for their low activation which is a high requirement for use in fusion reactors. Zr was chosen due to the larger negative enthalpy of mixing with other selected elements. The HEA showed increasing yield strength increased as temperatures were increased from below 500 °C. The yield strength was higher than of the vanadium alloy or martensitic steel developed for fusion applications when temperatures ranged from room temperature to 900 °C. At 700 °C, the paper reported that the yield strength of the HEA was about 500MPa higher than the vanadium alloy and martensitic steel showing great promise for first wall material application. Below 700 °C, the HEA showed a relatively low ductility while the ductility increased over 700 °C [38].

2.3.2   Radiation damage in high entropy alloys

A high priority property for first wall materials is the radiation behaviour in fusion reactors. The study here gives insight in the irradiation behaviour of HEAs including the fundamental research to investigate the irradiation-induced phase crystal structure change and volume swelling [39]. HEAs typically crystallize in a simple Body Centred Cubic (BCC) or Face Centred Cubic. BCC-type metals and alloys have a large capacity to store hydrogen due to their structure [44 – 46]. The presence of lattice strain within the lattice or at interfaces in some metals can be favourable for hydride Formation [43]. These two facts show that HEAs have a high amount of storage potential for hydrogen due to the lattice strain alone [44].

A typical feature from HEAs are their lattices which are distorted due to the variations in the atomic radii of the constituent atoms [44]. This kind of distortion will lead to a strained lattice which has the potential to be beneficial for hydride formation. However, there are problems with the lattice spacing in solid solutions. The lattice spacing shows a relationship between the percentage lattice distortion and the solute valency in binary systems. Metals like aluminium are able to show a contraction in lattice spacing by lithium and silicon, copper and zinc.

BSE images (Fig 7) of the alloys show a microstructure consisting of a light grey matrix with darker precipitates. The precipitates found in the ternary alloys (Fig 7 (a)–(d)) are a mixture of larger, more rounded shapes which appear along grain boundaries, and smaller long and thin precipitates that are intragranular. The matrix appeared as a single phase in all alloys. This was confirmed to be body centred cubic (BCC) (Å) through X-ray and TEM diffraction [4].
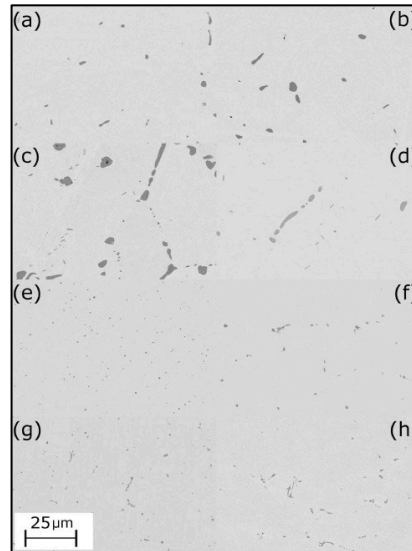
Figure 7 Representative BSE images of alloy (a) V–20Cr–20Mn (b) V–20Cr–40Mn (c) V–40Cr–20Mn (d) V–Cr–Mn (e) V–Cr–Mn–1%Ti (f) V–Cr–Mn–2%Ti (g) V–Cr–Mn–4%Ti (h) V–Cr–Mn–8%Ti. [76]

One of the main consequences of high energy radiation and damage processes associated with fusion reactions (including electrons, ions, neutrons, and photons) with materials, is the formation of defects within the lattice that occurs from the energy transfer to the atoms [43]. Other effects include production of non-damage-producing phonons, excitons and plasmons, secondary electrons and photons and heating of the material [43]. The damage can be perceived as either detrimental or beneficial due to them being able to take so many forms.

Within a crystal, the atom can be displaced from its initial lattice site which leaves a vacancy in its place while producing an atom at an interstitial site [45]. The types of damage to a crystal can take many forms; each with their own structures (often described as 1-, 2- and 3 dimensional). They can be 1-dimensional point defects, 3-dimensional defect clusters [46] and amorphous zones [47], [48], and 2-dimensional dislocation loops [49], or three-dimensional defects [19,20]. The damage can be recognised by two categories by time scale. The primary damage is first created immediately from the particle impact by atomic collision processes and strong material heating caused by the colliding atoms causing a great change in the thermodynamic equilibrium. The following can range from nano seconds to years where thermally activated damage evolves based on the primary knock-on atom (PKA) temperature, higher final thermalization temperature and exponentially increasing atomic mobility to thermally accelerate the evolution stage [50].

2.3.3   Thermal Stability

Studies made by Ao Xia *et al.* have reported on the thermal stability of the BCC high entropy alloy MoNbTaVW as solid solution thin films[51]. The material was synthesised by cathodic arc deposition. They found that after annealing up to 1600 °C, the thermal stability of the material is stable up to 1500 °C. With limited contamination with spots of emission droplets

from the high plasma pressure when interacting with the cathodes, the film remained relatively smooth. It was also noticed that with higher annealing temperatures of 1500 °C and above, the surface suffered some roughening, but it was noted that there was no of signs delamination. The concentrations of the constituting elements in the as-deposited state were measured between 18 and 22 at. % (representing the cathode composition). As annealing temperatures increased to 1400-1500 °C, vanadium content decreased to 10 at.%. When temperatures were raised to 1600 °C, severe film spalling occurred leaving no material to measure. The hardness of the film was measured to lower from ~19 to ~9 GPa after annealing in vacuum.

Overall, the thin film material showed promising thermal and mechanical properties. With it only being a thin film, it was able to show great thermal conductivity up to 1600 °C. The use of arc melting, and powder metallurgy was not seen as a suitable method of synthesis. If the material was composited as a more than a thin film, there may have been more margin to measure the composition of the material at higher temperatures. Due to the thin deposit of the material, the higher temperatures causing the film spalling meant there was no opportunity for measurements above 1600 °C. Temperatures were shown to vaporise vanadium 17 °C below the melting of tungsten which caused the concentration of vanadium to fall below the deposited amount. Analysis of the film didn't show obvious phases to provide evidence of it being a single-phase high entropy alloy. This means there is opportunity for grain boundary weaknesses. Plasma facing materials are in direct contact with extremely high temperature and subjected to harsh environmental forces. A material chosen as the first wall material must possess a high melting point [52] and high thermal conductivity [53] when considering temperature. Understanding the thermal stability can provide evidence on the performance of a chosen material in this specific application.

3. Modelling Methods

In this study, we investigate the intrinsic defect formation in the equiatomic BCC MoNbTaVW model alloy to begin to assess the radiation damage properties of this and similar HEAs.

This particular HEA composition is chosen for:
- the presence of tungsten which provides the benefits of high strength, which persists to high temperatures and good to neutron and ion radiation [54].
- that the use of vanadium, which Yin et al. determined to improve the strength of this due to its large misfit volume in crystalline structures. [55] [14].
- Xia A et al. demonstrated the thermal stability of this composition up to 1500°C which is ~400°C higher than pure tungsten's recrystallisation temperature [15].

Atomic scale simulation methods are used to develop and understand the defect behaviour in MoNbTaVW HEA. The behaviour and formation of intrinsic species is considered to aid understanding into the materials response to radiation.

3.1 Density Functional Theory simulations

This work employed density functional theory (DFT)[11,12], using the Vienna Ab initio Simulation Package (VASP) [17]. Simulations were performed under constant pressure, allowing the cell volume and shape to relax as well as the atomic positions. Methfessel-Paxton smearing [18] with a smearing width of 0.1 eV. Cut-off energy of plane waves were 500 eV. A 4×4×4 K-point mesh was used after ENCUT convergence testing of MoNbTaVW. The ENCUT value of 500 was used due to the total change in energy to be 0.1% after an increase of 50 eV. The generalised gradient approximation (GGA) exchange correlation was used as determined by Perdew Burke and Ernzerhof [19]. The pseudopotential library provided with VASP 5.4.4 was used.

Special quasi-random structures (SQS) [20] were used to produce ten 3×3×3 BCC supercells of MoNbTaVW containing 54 sites to which the alloy's elements were assigned (Fig 8 shows an example structure). In the perfect system, 11 of each element was included in the system apart from Ta that had 10 atoms present (totalling the 54 lattice sites in the system).
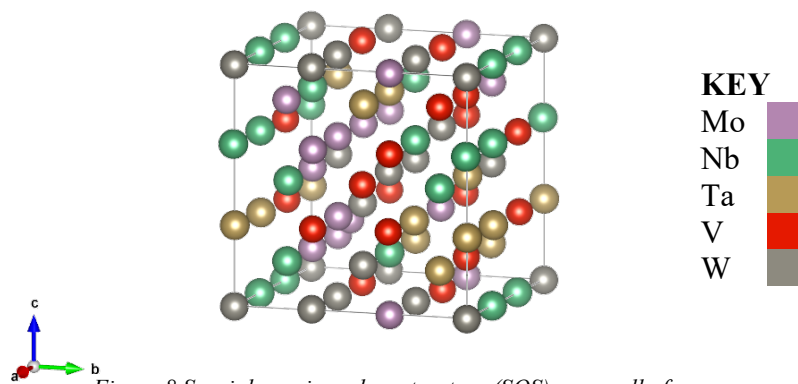
Figure 8 Special quasi-random structure (SQS) supercell of near equiatomic MoNbTaVW

KEY
Mo
Nb
Ta
V
W

Vacancy calculations were performed by removing a single atom to create a new 53-atom supercell. This method was repeated to produce 54 unique supercells. Similarly, isolated interstitials were considered in the HEA structure. Each perfect 54-atom supercell has a single atom added into predefined locations as interstitials to form a 55-atom supercell. Three interstitial sites were considered: the octahedral, tetrahedral and a crowdion arrangement. For each of these interstitial types, 10 different cells were generated per element. In total, 162 supercells with an interstitial containing 55 atoms were considered.

4. Results and discussion

4.1 Perfect Structure

SQS cells with the perfect structure were simulated where the lattice positions of the elements and lattice parameter of the cell was allowed to relax. Using 10 randomly arranged perfect cells (with the same concentration), the average lattice parameter at 0 K was computed to be 3.19 ± 0.01 Å. Byggmaster et al. calculated the MoNbTaVW lattice parameter at 3.195 ± 0.001Å [21]. Experiments showed a value 3.1832 Å [22].

Table 2 Calculated lattice parameters of 10 randomly arranged perfect cells

	Calculated Lattice Parameter
1	3.1907
2	3.1934
3	3.1901
4	3.1940
5	3.1939
6	3.1934
7	3.1965
8	3.1901
9	3.1944
10	3.1953
Average Å	3.1932
STDEV	0.0021945
ST ERROR	0.000694

The enthalpy of formation of the HEA with respect to the individual elements was computed to be -0.04 eV per atom (averaging over the 10 SQS structures produced). Proving exothermic, this highlights the stability of the alloy with respect to pure elements. Stability means low reactivity for the material providing energetically favourable reactions. Low reactivity can lead to a longer lifespan for the material due to lower surface damage which will create less contamination to the plasma from dust formations.

4.2 Defect Formations

Significant relaxation of interstitial defects was observed when inserting elements in as an octahedral interstitial. 74 % of the relaxed structures are split-interstitials during the energy minimisation process, where two interstitial species share a single lattice site. 70.3 % of the split interstitials were vanadium-vanadium split interstitials. Further inspection of the relaxed interstitial structures shows a distinct behaviour: 91.8 % of the relaxed interstitials involved a vanadium, either as part of a split-interstitial or crowdion [63] cluster, or as an isolated vanadium interstitial. The defect types are shown in table 3 and 4.

Table 3 Defect types found including formation energies and frequency.

Defect type	Defect Energy	Frequency
V-V	7.34 ± 0.08	26
V-Nb	8.98 ± 0.57	2
V-Ta	9.30 ± 0.44	2
V-W	8.52 ± 0.45	3
V-W-Ta	9.68 ± 0	1
OCT INT	7.94 ± 0.69	3
V-W-W-V	8.94 ± 0.36	2
V-W-Ta-V	7.82 ± 0	1
V-Mo	7.58 ± 0.32	3
V-Nb-Mo	7.51 ± 0.45	3
Nb-W	8.45 ± 0	1
V-Ta-V	8.16 ± 0.12	2
V-Mo-V	7.96 ± 0	1

Table 4 Defect types following with interstitials of different elements.

Type	Mo	Nb	Ta	V	W
Split	8	7	8	8	6
Crowdion	2	3	2	0	3
Interstitial	0	0	0	2	1

Table 4 shows that majority of the defects found are split interstitials. However, the element that was added as the initial interstitial showed no correlation in the frequency of defects that occurred. This was expected as often pure BCC structures introduced with interstitials, form split interstitials as they are considered a stable defect. As the material in study was not pure, it was expected to see more split interstitials to form due to varying sizes of atoms.

Calculated from a matrix of each 10 perfect cells and 10 vacancy cells with the corresponding element, Table 5 shows the total of 500 calculations made to each simulated vacancy cell to give the average vanacy formation energy. The vacancy formation energy (E_{Vac}) is given by [23] :

$$E_{Vac} = E_{Defective} + E_{Metal} - E_{Perfect} \qquad \text{Eq (2)}$$

where a system containing a vacancy ($E_{Defective}$) was created forming its individual metal (E_{Metal}) from a perfect supercell ($E_{Perfect}$). The relaxed structures showed simple vacancy defects formed in each case (no evidence of split vacancies or extensive restructuring). Table 5 reports the vacancy formation energies computed for each species forming a unit of its metal (in each case energies were generated for the perfect BCC metal). For comparison, the table provides the vacancy formation energies of each type in the pure metals. The standard error was calculated by taking the mean of the errors associated with each vacancy formation energy for each element.

To understand thermal dynamic properties of a material, looking into the vacancies behaviour and atom mobility is necessary to interpret the behaviour of a metal. Focus on vacancy formation energy determines the mobility when a material is subjected to energies or radiation. T. Korhonen *et al.* focuses on performing first-principal total-energy calculations in a series of BCC and FCC transition metals using full-potential linear-muffin-tin-orbital method [53].

Table 5 Average vacancy formation energy

Element	Average vacancy formation energy	Standard deviation
Mo	3.67	0.25
Nb	3.33	0.22
Ta	3.55	0.33
V	3.43	0.15
W	3.48	0.30
Average	**3.49**	

Another matrix of each 10 perfect cells, 10 vacancy cells and 10 of each interstitial cell with the corresponding element. This made a total of 500 calculations to calculate an average Frenkel Pair formation energy shown in Table 6. Frenkel pair energy was given by:

$$E_{Frenkel\ pair} = E_{Interstitial} + E_{Vacancy} - 2(E_{Perfect}) \qquad \text{Eq (3)}$$

Table 6 Average Frenkel Pair energy

Element	Average Frenkel Pair energy	Standard deviation
Mo	7.84	1.01
Nb	7.69	0.90
Ta	7.83	0.86
V	7.21	0.40
W	8.10	1.12
Average	7.73	

Table 7 shows the calculated average Frenkel energy from this experiment against calculations made by (*Ma P, Dudarev S, 2019*) of the same elements but in isolated pure systems. Average Frenkel pair energies showed a 4.7eV (13.13%) increase for the HEA compared to the pure systems. This shows how the HEA requires more energy to form Frenkel pairs that forces atoms off their sites. This could lead to a higher resistance to neutron and ion radiation. However, increases in system energy also increases instability.

Table 7 Average Frenkel pair energy of pure systems compared to experimental HEA system

Element	Tetra [65]	Octa[65]	Average	Experiment	Difference
Mo	8.358	8.916	8.637	7.84	-0.79
Nb	4.422	4.618	4.52	7.69	3.17
Ta	5.770	5.946	5.858	7.83	1.97
V	2.898	2.895	2.8965	7.21	4.31
W	11.717	12.265	11.991	8.10	-3.89
					4.76

A matrix of each 10 perfect cells against 10 interstitial cells with the corresponding element to make a total of 500 calculations forming an average of each simulated interstitial cell (Table 8). Interstitial energy was given by:

$$E_{Int\ formation} = E_{Interstitial} + E_{Metal} - E_{Perfect} \qquad \text{Eq (4)}$$

Table 8 Average interstitial formation energy

Element	Average interstitial formation energy	Standard deviation
Mo	3.64	0.95
Nb	3.31	0.88
Ta	3.52	0.86
V	3.41	0.41
W	3.45	1.02
Average	3.47	

The predicted interstitial formation energies in this HEA are higher than those reported in the individual metal systems when compared to previously published work including that of Korhonen *et al.* [25], indicating a deviation in the expected behaviour, potentially resulting from a change in bonding in the system, possibly associated with intermetallic compounds. A Schotty defect energy (Es) in a metal is the energy required to create a vacancy producing a unit of material [67]. The equation used in this thesis to compute the Schottky energy is defined as:

$$E_S = E_{Supercell\ with\ vacancy} - E_{Perfect\ Supercell} - E_{Unit\ of\ material\ removed\ from\ vacancy}$$
$$\text{Eq (5)}$$

The Schottky energy calculated in this high entropy alloy is similar to the Schottky energy calculated for W and Ta [68].

The calculations made for the structures [66] were presented based on DFT within local-density approximation (LDA) shown in table 9. The use of fill non-sphericity of charge density was found to be essential for accurate vacancy formation energies. Meshes ranged from 16 to 10 K-points for BCC and FCC supercells, respectively. There was six bcc (V, Cr, Nb, Mo, Ta, W) and six fcc (Ni, Cu, Pd, Ag, Pt, Au) used for the experiment. FP-LMTO-LDA was shown to underestimate the lattice constants in the biggening of 3d series as a well-known deficit of LDA. Results showed that the FP-LMTO-GGA values agreed with experimental data even though on average, it did show the highest lattice constraints compared to other data used in the experiment as GGA is expected to overestimate. However, it was shown that the calculated vacancy formation energies increase at the beginning of the *d* series and decrease at the end following the general trend from cohesion and surface energies.

Table 9 Vacancy formation energy of pure elements with previous FP-LMTO experimental and DFT experimental values. Supercells size for simulated DFT of N=54 and FP-LMTO N=27 with BCC metals.

Element	Average Vacancy Formation Energy (eV)	Vacancy in monoatomic metal (eV)
Mo	3.67 ± 0.25	2.61[24], 3.13[25]
Nb	3.33 ± 0.23	2.31[26], 2.92[25]
Ta	3.54 ± 0.34	3.49[25]
V	3.43 ± 0.15	3.06[25]
W	3.48 ± 0.29	2.95[27], 3.27[25]

[24] *Einstein crystal method*
[25] *Density functional theory within the LDA*
[26] *Density functional theory (generalized gradient approximation of Perdew and Wang (PW91))*
[27] *DFT exchange correlation functional GGA-PBE calculations*

It is noted that atomic-sphere approximation (ASA) from the LDA experiment does not give reliable total energies for defects although the structural properties of the bulk items were quite reasonable. They only simulated two cells with small supercells with 27 lattice sites for BCC and 32 for FCC supercells. The sample size for the calculations may not necessarily consider multiple configurations for a randomly distributed cell which would give indications of the behaviour of atoms with various nearest neighbours.

To predict the vacancy formation energy for each element, simulations using the same DFT methods for pure element cells were made to provide the free enthalpy energy of a single atom. Results shown in table 10.

Table 10 Energy of cells containing pure elements.

Element	Free Energy (eV)
Mo	-10.96
Nb	-10.21
Ta	-11.86
V	-9.13
W	-13.01

Figure 9 illustrates a typical simulation that highlights how a tantalum atom added to an octahedral site displaces an adjacent vanadium atom out of its lattice site to form a split interstitial. As can be seen, the atom identified as Ta moves onto a site previously occupied by a vanadium which forms a split-interstitial with another vanadium.
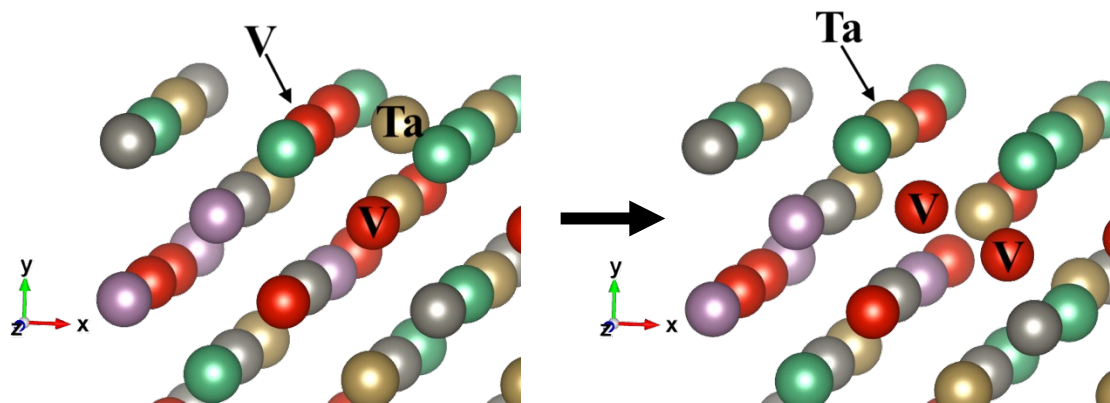
Figure 9 Relaxation forming a split interstitial made of two vanadium atoms after a tantalum atom was placed as an interstitial defect.

This barrierless restructuring of interstitial defects highlights a key, distinct behaviour difference between these HEAs and more standard alloys that will not only impact the defect population in the material, but also the recombination volume of the defects (which will aid defect recovery).

By considering the vacancy and interstitial defects together, the isolated Frenkel formation energy can be computed. Accommodation mechanisms for the additional atoms were compared in Fig 12. The Frenkel formation energy averaged for each defect that formed, and the frequency of each defect as a percentage of those observed is reported. As can be expected, the V-V split interstitial that was observed to form more frequently is also predicted to be most favourable with an average of 7.34 eV $\pm$ 0.42.

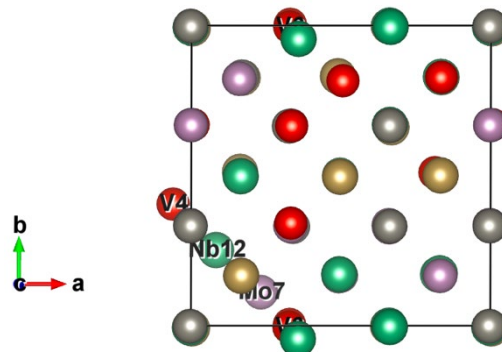*Figure 10 Crowdion defect after niobium atom added as interstitial.*

Defects formed from a niobium atom added as an interstitial in fig 10 shows a formation of a crowdion defect. The defect energy for this specific formation to occur was calculated at 7.07eV; 15% lower than the average energy for all defects recorded. Being lower than average, it is expected to be a more desirable defect to occur however crowdion defects have been less frequent than the split interstitials found. Compared to split interstitials that didn't contain vanadium (the highest mobile element), there are 10 crowdion defects compared to the 4 split interstitials left making them the most desirable defect to occur. Future work can consider larger systems sizes to understand the impact of system size on crowdion defect stability versus split interstitials.

When adding a vanadium atom as an interstitial, the atom remained at the initially placed site after relaxation. With a defect formation energy of just 7.55eV, this remained 9.2% lower than the average making it a more desirable defect to occur. With vanadium being the smallest element in the system, its ability to displace other constituent atoms bigger than itself is less likely.
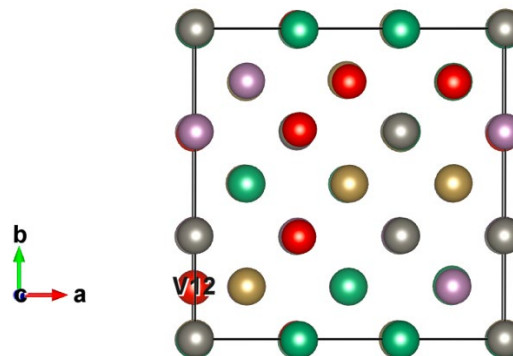

Figure 11 Vanadium added as interstitial remained at site after relaxation.
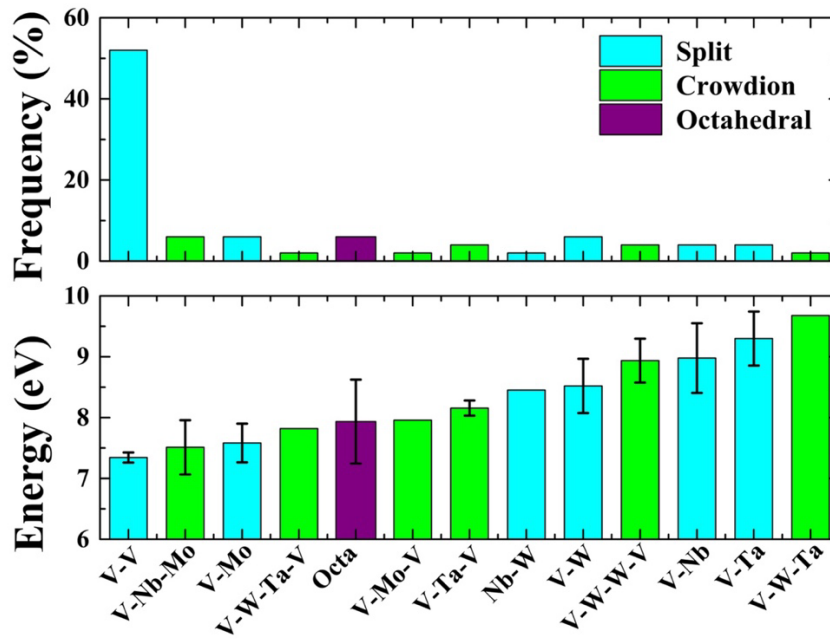
Figure 12 Average defect formation energy of every observed defect after relaxation. The standard error has been calculated for each defect type observed. Defects only observed once have no error bar associated with them.

In a similar manner to the computation of the Schottky energy, the anti-Schottky energy was computed (taking a unit of HEA and accommodating it as interstitial defects) [67]. The anti-Schottky energy is computed to be 3.79 eV. This value is similar to that of the computed Schottky energy (3.48 eV ± 0.27). Due to the Schottky energy being lower than the anti-Schottky, we know that the formation of a Schottky defect is more desirable.

Within a tokamak, the first wall material will be irradiated with neutrons and ions. The HEA has shown a higher Frenkel pair formation energy when compared to the same elements in isolated systems. This provides us with insight in the energy tolerance of the material when irradiated with neutron or ion radiation. For a first wall material, high defect formation energies are somewhat desirable as more energy is required to be moved off their sites thus a higher resistance to produce the same population of defects. Further, there will be a higher thermodynamic drive for individual defect recombination. However, it has been shown that once the defect formation has occurred, there is also the potential for clustering of defects and dislocation formation. In metals, this has great impact on mechanical behaviour, often creating a more brittle system [72]. It is also recognised how the material forms an exothermic reaction in the simulated environment. This reaction indicates how the material is particularly stable allowing higher resistance to corrosion. The high mobility of vanadium within the HEA and the formation of the split interstitials may be the cause to the reported strengthening by Yin *et al.* [27]. While the material is irradiated more and creating more defects, there are an increase in these split interstitials forming a potentially stronger material over time.

5. Summary

To conclude, the intrinsic defect behaviour in the MoNbTaVW HEA has been assessed and distinct differences are observed when compared to simple metals such as tungsten. The key findings are as follows:

- The most favoured intrinsic defect is predicted to be the Schottky defect with a formation energy of 3.48 eV ± 0.27. The predicted concentration of vacancies under equilibrium conditions could be expected to be similar to that of W, which shares a similar Schottky energy [27].
- The anti-Schottky energy (forming interstitials) has a similar energy in this HEA: 3.79 eV.
- Frenkel pair formation is predicted to be less favourable than both the Schottky and anti-Schottky energies under equilibrium conditions (with formation energies >7 eV).
- When interstitial defects were considered, a clear preference for the formation of split interstitial defects was observed.
- Vanadium was the most common defect specie and the most energetically favourable in all split interstitial defects observed, often forming when other interstitial defects were originally placed into the structure. Vanadium is the metal with the smallest atomic radius in the composition considered, which may explain the observations (causing less steric disturbance). Vanadium is described as a great strengthening addition to HEAs by Yin *et al.* [27]. The preferential formation of split interstitials and other defects containing this element may be the cause of this strengthening, impacting the behaviour of dislocations in the material.
- Interstitials have been observed to displace and migrate with no energy barrier, highlighting that the recombination volume of interstitials is expected to be larger compared to a standard alloy composed of a single principal element.

6. Future work

During the research, the limitations of technology has restricted the simulations for such large-scale computations. Fabricating this high entropy alloy with the supporting predictions of the research, a physical material to test can give real-world insight on how it behaves under irradiation. Due to the high recombination volume of this material compared to alloys made of the similar alloy composed of a singular principal element, physical research could characterise the material behaviour with these supporting results.

Due to the impacts of neutron and ion irradiation, there are high chances of transmutation due to changes in the nucleus of atoms. With a manufactured composition that has specific concentrations of elements to possess the desired properties for application, changes in the elements through transmutation may have impacts on the behaviour of the material.

The harsh environment that the first wall material will be subjected will develop impurities. Impacts of the hydrogen rich exposure could lead to blistering to the first wall. The size of the blistering and the frequency will give an understanding on possible dust formation. This will be essential information as dust is a contaminate to the plasma that can impact the efficiency of the reactions. The dust will also be a source of waste that must be minimised.

From the research conducted, results showed defects from neutron and ion irradiation that provided a clear preference for split interstitial formation. Due to the smaller size of vanadium compared to the constituent atoms within the system, an understanding on how the effects of this process can affect a material at a larger scale may help with forming stronger evidence on the behaviour of this high entropy alloy. To do this, perform molecular dynamic cascades to access defect formations at a larger scale. Beginning with simulations of supercells with a larger quantity of atoms and inserting multiple vacancies and interstitials into the same cell to relax, could give an understanding on possible cascade events. Simulating multiple steps with a selection of different defects could allow for greater understanding on chain events at a larger scale.

7. References

[1]   J. W. Yeh *et al.*, "Nanostructured High-Entropy Alloys with Multiple Principal Elements: Novel Alloy Design Concepts and Outcomes," *Advanced Engineering Materials*, vol. 6, no. 5, pp. 299–303, May 2004, doi: 10.1002/ADEM.200300567.

[2]   J. Yeh, "Recent progress in high-entropy alloys," *Ann. Chim. Sci. Des Matéraux*, vol. 31, no. 6, p. 633, Nov. 2006, doi: 10.3166/acsm.31.633-648.

[3]   J. W. Yeh, "Alloy design strategies and future trends in high-entropy alloys," *JOM*, vol. 65, no. 12, pp. 1759–1771, Dec. 2013, doi: 10.1007/S11837-013-0761-6/FIGURES/12.

[4]   D. B. Miracle, "Exploration and development of high entropy alloys for structural applications," *Entropy*, vol. 16, no. 1, p. 498, 2014, doi: 10.3390/e16010494.

[5]   Y. K. M. Peng and D. J. Strickler, "Features of spherical torus plasmas," *Nuclear Fusion*, vol. 26, no. 6, pp. 769–777, 1986, doi: 10.1088/0029-5515/26/6/005.

[6]   A. Sykes, "The spherical tokamak programme at Culham," *Nuclear Fusion*, vol. 39, no. 9Y, p. 1271, Sep. 1999, doi: 10.1088/0029-5515/39/9Y/305.

[7]   A. Sykes *et al.*, "Compact fusion energy based on the spherical tokamak," *Nuclear Fusion*, vol. 58, no. 1, p. 016039, Nov. 2017, doi: 10.1088/1741-4326/AA8C8D.

[8]   D. Clery, "The new shape of fusion," *Science (1979)*, vol. 348, no. 6237, pp. 854–856, May 2015, doi: 10.1126/science.348.6237.854

[9]   B. N. Sorbom *et al.*, "ARC: A compact, high-field, fusion nuclear science facility and demonstration power plant with demountable magnets," *Fusion Engineering and Design*, vol. 100, pp. 378–405, Nov. 2015, doi: 10.1016/J.FUSENGDES.2015.07.008.

[10]   "Development of advanced high heat flux and plasma-facing materials," 2017, doi: 10.1088/1741-4326/aa6f71.

[11]   "5 Big Ideas for Making Fusion Power a Reality - IEEE Spectrum." https://spectrum.ieee.org/5-big-ideas-for-making-fusion-power-a-reality (accessed Dec. 10, 2021).

[12]   J. T. Hogan, "The accessibility of high-beta tokamak states," *Nuclear Fusion*, vol. 19, no. 6, p. 753, Jun. 1979, doi: 10.1088/0029-5515/19/6/006.

[13]   V. A. Vershkov and S. v. Mirnov, "Role of impurities in current tokamak experiments," *Nuclear Fusion*, vol. 14, no. 3, p. 383, Jun. 1974, doi: 10.1088/0029-5515/14/3/012.

[14]   R. A. Causey, "Hydrogen isotope retention and recycling in fusion reactor plasma-facing components," *Journal of Nuclear Materials*, vol. 300, no. 2–3, pp. 91–117, Feb. 2002, doi: 10.1016/S0022-3115(01)00732-2.

[15]   M. Kaufmann and R. Neu, "Tungsten as first wall material in fusion devices," *undefined*, vol. 82, no. 5–14, pp. 521–527, Oct. 2007, doi: 10.1016/J.FUSENGDES.2007.03.045.

[16]   R. A. Pitts *et al.*, "Material erosion and migration in tokamaks," *Plasma physics and controlled fusion 47*, 2005.

[17]   J. P. Coad *et al.*, "Erosion/deposition issues at JET," *Journal of Nuclear Materials*, vol. 290–293, pp. 224–230, Mar. 2001, doi: 10.1016/S0022-3115(00)00479-7.

[18]   H. Bolt *et al.*, "Plasma facing and high heat flux materials – needs for ITER and beyond," *Journal of Nuclear Materials*, vol. 307–311, no. 1 SUPPL., pp. 43–52, Dec. 2002, doi: 10.1016/S0022-3115(02)01175-3.

[19]   H. Maier, J. Luthin, M. Balden, J. Linke, F. Koch, and H. Bolt, "Properties of tungsten coatings deposited onto the fine grain graphite by different methods," *Surface and Coatings Technology*, vol. 142–144, pp. 733–737, Jul. 2001, doi: 10.1016/S0257-8972(01)01177-X.

[20] Masayuki Ono, "Lithium As Plasma Lithium as Plasma Facing Component For Magnetic Fusion Research facing Component For Magnetic Fusion Research," *Princeton Plasma Physics Lab.(PPPL)*, 2012.

[21] C. P. C. Wong, "Innovative tokamak DEMO first wall and divertor material concepts," *Journal of Nuclear Materials*, vol. Complete, no. 390–391, pp. 1026–1028, Jun. 2009, doi: 10.1016/J.JNUCMAT.2009.01.274.

[22] D. Nishijima, M. Y. Ye, N. Ohno, and S. Takamura, "Formation mechanism of bubbles and holes on tungsten surface with low-energy and high-flux helium plasma irradiation in NAGDIS-II," *Journal of Nuclear Materials*, vol. 329–333, no. 1-3 PART B, pp. 1029–1033, Aug. 2004, doi: 10.1016/J.JNUCMAT.2004.04.129.

[23] J. B. Keith, H. Wang, B. Fultz, and J. P. Lewis, "Ab initio free energy of vacancy formation and mass-action kinetics in vis-active TiO2," *Journal of Physics Condensed Matter*, vol. 20, no. 2, Jan. 2008, doi: 10.1088/0953-8984/20/02/022202.

[24] K. M. Youssef, A. J. Zaddach, C. Niu, D. L. Irving, and C. C. Koch, "A Novel Low-Density, High-Hardness, High-entropy Alloy with Close-packed Single-phase Nanocrystalline Structures," *http://mc.manuscriptcentral.com/tmrl*, vol. 3, no. 2, pp. 95–99, Dec. 2014, doi: 10.1080/21663831.2014.985855.

[25] Z. J. Zhang *et al.*, "Nanoscale origins of the damage tolerance of the high-entropy alloy CrMnFeCoNi," *Nat Commun*, vol. 6, Dec. 2015, doi: 10.1038/NCOMMS10143.

[26] N. A. P. K. Kumar, C. Li, K. J. Leonard, H. Bei, and S. J. Zinkle, "Microstructural stability and mechanical behavior of FeNiMnCr high entropy alloy under ion irradiation," *Acta Materialia*, vol. 113, no. C, pp. 230–244, May 2016, doi: 10.1016/J.ACTAMAT.2016.05.007.

[27] S. A. Rice, "Article in Physics Today," 1963, doi: 10.1063/1.3050727.

[28] B. Fultz, "Vibrational thermodynamics of materials," *Progress in Materials Science*, vol. 55, no. 4, pp. 247–352, May 2010, doi: 10.1016/J.PMATSCI.2009.05.002.

[29] J. W. Yeh *et al.*, "Nanostructured High-Entropy Alloys with Multiple Principal Elements: Novel Alloy Design Concepts and Outcomes," *Advanced Engineering Materials*, vol. 6, no. 5, pp. 299–303, May 2004, doi: 10.1002/ADEM.200300567.

[30] M. H. Tsai and J. W. Yeh, "High-entropy alloys: A critical review," *Materials Research Letters*, vol. 2, no. 3, pp. 107–123, 2014, doi: 10.1080/21663831.2014.912690.

[31] A. D. Pogrebnjak *et al.*, "Irradiation resistance, microstructure and mechanical properties of nanostructured (TiZrHfVNbTa)N coatings," 2016, doi: 10.1016/j.jallcom.2016.04.064.

[32] A. D. Pogrebnjak *et al.*, "Microstructure, physical and chemical properties of nanostructured (Ti-Hf-Zr-V-Nb)N coatings under different deposition conditions," *Materials Chemistry and Physics*, vol. 147, no. 3, pp. 1079–1091, Oct. 2014, doi: 10.1016/J.MATCHEMPHYS.2014.06.062.

[33] A. D. Pogrebnjak *et al.*, "Influence of residual pressure and ion implantation on the structure, elemental composition, and properties of (TiZrAlYNb)N nitrides," *Technical Physics 2015 60:8*, vol. 60, no. 8, pp. 1176–1183, Aug. 2015, doi: 10.1134/S1063784215080228.

[34] "The Differences Between Heat-Treatable and Non-Heat-Treatable Aluminum Alloys." http://www.alcotec.com/us/en/education/knowledge/qa/The-Differences-Between-Heat-Treatable-and-Non-Heat-Treatable-Aluminum-Alloys.cfm (accessed Dec. 31, 2021).

[35] X. Yang and Y. Zhang, "Prediction of high-entropy stabilized solid-solution in multi-component alloys," *Materials Chemistry and Physics*, vol. 132, no. 2–3, pp. 233–238, Feb. 2012, doi: 10.1016/J.MATCHEMPHYS.2011.11.021.

[36]   Y. Zhang, Y. J. Zhou, J. P. Lin, G. L. Chen, and P. K. Liaw, "Solid-Solution Phase Formation Rules for Multi-component Alloys," *Advanced Engineering Materials*, vol. 10, no. 6, pp. 534–538, Jun. 2008, doi: 10.1002/ADEM.200700240.

[37]   Z. Wang, Y. Huang, Y. Yang, J. Wang, and C. T. Liu, "Atomic-size effect and solid solubility of multicomponent alloys," *Scripta Materialia*, vol. 94, pp. 28–31, Jan. 2015, doi: 10.1016/J.SCRIPTAMAT.2014.09.010.

[38]   X. Xian *et al.*, "A high-entropy V35Ti35Fe15Cr10Zr5 alloy with excellent high-temperature strength," *Materials and Design*, vol. 121, pp. 229–236, May 2017, doi: 10.1016/J.MATDES.2017.02.029.

[39]   S. qin Xia, Z. Wang, T. fei Yang, and Y. Zhang, "Irradiation Behavior in High Entropy Alloys," *Journal of Iron and Steel Research, International*, vol. 22, no. 10, pp. 879–884, Oct. 2015, doi: 10.1016/S1006-706X(15)30084-4.

[40]   E. Akiba and Y. Nakamura, "Hydrogenation properties and crystal structures of Ti-Mn-V BCC solid solution alloys," *Metals and Materials International*, vol. 7, no. 2, pp. 165–168, 2001, doi: 10.1007/BF03026955.

[41]   E. Akiba and H. Iba, "Hydrogen absorption by Laves phase related BCC solid solution," *Intermetallics (Barking)*, vol. 6, no. 6, pp. 461–470, Jan. 1998, doi: 10.1016/S0966-9795(97)00088-5.

[42]   B. Sakintuna, F. Lamari-Darkrim, and M. Hirscher, "Metal hydride materials for solid hydrogen storage: A review," *International Journal of Hydrogen Energy*, vol. 32, pp. 1121–1140, 2007, doi: 10.1016/j.ijhydene.2006.11.022.

[43]   T.B. MASSALSKI, "structure and stability in alloys," *Physical Metallurgy (Fourth Edition)*, 1996.

[44]   M. Sahlberg, D. Karlsson, C. Zlotea, and U. Jansson, "Superior hydrogen storage in high entropy alloys," *Scientific Reports 2016 6:1*, vol. 6, no. 1, pp. 1–6, Nov. 2016, doi: 10.1038/srep36770.

[45]   Charles. Kittel, "Introduction to solid state physics," p. 680, 2005.

[46]   K. Nordlund, P. Partyka, Y. Zhong, R. S. Averback, I. M. Robinson, and P. Ehrhart, "Grazing incidence diffuse x-ray scattering investigation of the properties of irradiation-induced point defects in silicon," *Physical Review B*, vol. 64, no. 23, p. 235207, Nov. 2001, doi: 10.1103/PhysRevB.64.235207.

[47]   L. M. Wang *et al.*, "Irradiation-induced nanostructures," *Materials Science and Engineering: A*, vol. 286, no. 1, pp. 72–80, Jun. 2000, doi: 10.1016/S0921-5093(00)00677-8.

[48]   M. O. Ruault, J. Chaumont, J. M. Penisson, and A. Bourret, "High resolution and in situ investigation of defects in Bi-irradiated Si," *http://dx.doi.org/10.1080/01418618408237526*, vol. 50, no. 5, pp. 667–675, 2011, doi: 10.1080/01418618408237526.

[49]   B. L. Eyre, "Transmission electron microscope studies of point defect clusters in fcc and bcc metals," *Journal of Physics F: Metal Physics*, vol. 3, no. 2, p. 422, Feb. 1973, doi: 10.1088/0305-4608/3/2/009.

[50]   K. Nordlund *et al.*, "Primary radiation damage: A review of current understanding and models," *Journal of Nuclear Materials*, vol. 512, pp. 450–479, Dec. 2018, doi: 10.1016/J.JNUCMAT.2018.10.027.

[51]   A. Xia and R. Franz, "Thermal stability of monbtavw high entropy alloy thin films," *Coatings*, vol. 10, no. 10, pp. 1–8, Oct. 2020, doi: 10.3390/COATINGS10100941.

[52]   R. A. Johnson, "Point-defect calculations for tungsten," *Physical Review B*, vol. 27, no. 4, p. 2014, Feb. 1983, doi: 10.1103/PhysRevB.27.2014.

[53] T. Korhonen, M. J. Puska, and R. M. Nieminen, "Vacancy-formation energies for fcc and bcc transition metals," *Physical Review B*, vol. 51, no. 15, p. 9526, Apr. 1995, doi: 10.1103/PhysRevB.51.9526.

[54] O. El-Atwani *et al.*, "Outstanding radiation resistance of tungsten-based high-entropy alloys," *Science Advances*, vol. 5, no. 3, 2019, doi: 10.1126/SCIADV.AAV2002.

[55] B. Yin, F. Maresca, and W. Curtin, "Vanadium is an optimal element for strengthening in both fcc and bcc high-entropy alloys," *Acta Materialia*, vol. 188, pp. 486–491, Apr. 2020, doi: 10.1016/J.ACTAMAT.2020.01.062.

[56] G. Kresse and J. Furthmüller, "Efficiency of ab-initio total energy calculations for metals and semiconductors using a plane-wave basis set," *Computational Materials Science*, vol. 6, no. 1, pp. 15–50, Jul. 1996, doi: 10.1016/0927-0256(96)00008-0.

[57] G. Kresse and J. Hafner, "*Ab initio* molecular dynamics for liquid metals," *Physical Review B*, vol. 47, no. 1, p. 558, Jan. 1993, doi: 10.1103/PhysRevB.47.558.

[58] G. Y. Huang, N. Juslin, and B. D. Wirth, "First-principles study of vacancy, interstitial, noble gas atom interstitial and vacancy clusters in bcc-W," *Computational Materials Science*, vol. 123, pp. 121–130, Oct. 2016, doi: 10.1016/J.COMMATSCI.2016.06.022.

[59] B. Hammer, L. B. Hansen, and J. K. Nørskov, "Improved adsorption energetics within density-functional theory using revised Perdew-Burke-Ernzerhof functionals," *Physical Review B*, vol. 59, no. 11, p. 7413, Mar. 1999, doi: 10.1103/PhysRevB.59.7413.

[60] A. Zunger, S.-H. Wei, L. G. Ferreira, and J. E. Bernard, "Special quasirandom structures," *Physical Review Letters*, vol. 65, no. 3, p. 353, Jul. 1990, doi: 10.1103/PhysRevLett.65.353.

[61] J. Byggmästar, K. Nordlund, and F. Djurabekova, "Modeling refractory high-entropy alloys with efficient machine-learned interatomic potentials: defects and segregation," *Physical Review B*, vol. 104, no. 10, Jun. 2021, doi: 10.1103/physrevb.104.104101.

[62] O. N. Senkov, G. B. Wilks, J. M. Scott, and D. B. Miracle, "Mechanical properties of Nb25Mo25Ta25W25 and V20Nb20Mo20Ta20W20 refractory high entropy alloys," *Intermetallics (Barking)*, vol. 19, no. 5, pp. 698–706, May 2011, doi: 10.1016/J.INTERMET.2011.01.004.

[63] S. P. Fitzgerald and D. Nguyen-Manh, "Peierls potential for crowdions in the bcc transition metals," *Physical Review Letters*, vol. 101, no. 11, p. 115504, Sep. 2008, doi: 10.1103/PHYSREVLETT.101.115504/FIGURES/2/MEDIUM.

[64] Y. Pan and Y. Lin, "Influence of vacancy on the mechanical and thermodynamic properties of IrAl3 compound: A first-principles calculations," *Journal of Alloys and Compounds*, vol. 684, pp. 171–176, Nov. 2016, doi: 10.1016/J.JALLCOM.2016.05.173.

[65] P.-W. Ma and S. L. Dudarev, "Universality of point defect structure in body-centered cubic metals," 2019, doi: 10.1103/PhysRevMaterials.3.013605.

[66] T. Korhonen, M. J. Puska, and R. M. Nieminen, "Vacancy-formation energies for fcc and bcc transition metals," *PHYSICAL REVIEW B*, vol. 51, pp. 15–1995, 1994, doi: 10.1103/physrevb.51.9526.

[67] S. C. Middleburgh and R. W. Grimes, "Defects and transport processes in beryllium," *Acta Materialia*, vol. 59, no. 18, pp. 7095–7103, Oct. 2011, doi: 10.1016/J.ACTAMAT.2011.07.064.

[68] X. Lv, W. Wei, P. Zhao, J. Li, B. Huang, and Y. Dai, "Tunable Schottky contacts in MSe2/NbSe2 (M = Mo and W) heterostructures and promising application potential in field-effect transistors," *Physical Chemistry Chemical Physics*, vol. 20, no. 3, pp. 1897–1903, Jan. 2018, doi: 10.1039/C7CP07546D.

[69]   G. S. Smirnov and V. v. Stegailov, "Formation free energies of point defects and thermal expansion of bcc U and Mo," *Journal of Physics: Condensed Matter*, vol. 31, no. 23, p. 235704, Apr. 2019, doi: 10.1088/1361-648X/AB0E31.

[70]   A.-Y. Gao, Y.-L. Liu, Z.-H. Dai, and C. Duan, "Elucidating hydrogen assisting vacancy formation in metals: Mo and Nb as examples," *Eur. Phys. J. B*, vol. 86, p. 355, 2013, doi: 10.1140/epjb/e2013-40552-x.

[71]   S. C. Middleburgh, R. E. Voskoboinikov, M. C. Guenette, and D. P. Riley, "Hydrogen induced vacancy formation in tungsten," *Journal of Nuclear Materials*, vol. 448, no. 1–3, pp. 270–275, May 2014, doi: 10.1016/J.JNUCMAT.2014.02.014.

[72]   J. Spitaler and S. K. Estreicher, "Perspectives on the theory of defects," *Frontiers in Materials*, vol. 5, p. 70, Dec. 2018, doi: 10.3389/FMATS.2018.00070/BIBTEX.

[73]   B. Yin, F. Maresca, and W. A. Curtin, "Vanadium is an optimal element for strengthening in both fcc and bcc high-entropy alloys," *Acta Materialia*, vol. 188, pp. 486–491, Apr. 2020, doi: 10.1016/J.ACTAMAT.2020.01.062.

[74]   J. Hong *et al.*, "Exploring atomic defects in molybdenum disulphide monolayers," *Nature Communications*, vol. 6, 2015, doi: 10.1038/NCOMMS7293.

[75]   Z. Li, S. Zhao, R. O. Ritchie, and M. A. Meyers, "Mechanical properties of high-entropy alloys with emphasis on face-centered cubic alloys," *Progress in Materials Science*, vol. 102, pp. 296–345, May 2019, doi: 10.1016/J.PMATSCI.2018.12.003.

[76]   P. J. Barron, A. W. Carruthers, J. W. Fellowes, N. G. Jones, H. Dawson, and E. J. Pickering, "Towards V-based high-entropy alloys for nuclear fusion applications," *Scripta Materialia*, vol. 176, pp. 12–16, Feb. 2020, doi: 10.1016/J.SCRIPTAMAT.2019.09.028.